Supporting Information

Exploring the dicationic gemini surfactant for the generation of mesopores: A step towards the construction of hierarchical metal organic framework

Poonam Rani and Rajendra Srivastava*

Department of Chemistry, Indian Institute of Technology Ropar, Rupnagar-140001, India

*E-mail: rajendra@iitrpr.ac.in, Phone: +91-1881-242175; Fax: +91-1881-223395

Catalyst characterization

X-ray diffraction (XRD) patterns were recorded in the 2θ range of 5–50° with a scan speed of 2°/min on a PANalytical X'PERT PRO diffractometer, using Cu Kα radiation (λ=0.1542 nm, 40 kV, 40 mA). Nitrogen adsorption measurements were performed at 77 K by Quantachrome Instruments, Autosorb-IQ volumetric adsorption analyzer. Sample was out-gassed at 150 °C for 3 h in the degas port of the adsorption apparatus. The specific surface area was calculated from the adsorption branch using the Brunauer-Emmett-Teller (BET) equation. The pore diameter was estimated using non-local density functional theory (NLDFT) and Barret–Joyner–Halenda (BJH) method. Scanning electron microscopy measurements (SEM) were carried out on a JEOL JSM-6610LV to investigate the morphology and chemical composition of the MOF. The surface morphology was recorded by a field emission scanning electron microscope (FESEM, Quanta 200, Zeiss).Structural analysis of the as prepared samples were carried out by TEM using Jeol, JEM-1400 Plus. The sample was dispersed in hexane using ultrasonic bath, drop cost on a carbon coated Cu grid, dried, and used for TEM measurements. Fourier transform infrared (FTIR) spectra were recorded on a Bruker spectrophotometer in the region 400–4000 cm^{-1} (spectral resolution = 4 cm^{-1}; number of scans = 100). Thermo gravimetric analysis (TGA) was performed in the range of 25-600 °C on a TGA/DSC 1 STAR^{e} SYSTEM from Mettler Toledo, Switzerland, with temperature increments of 10 °C /min in N_2 atmosphere.

Table S1. Molar composition of micro and micro-mesopore MOF

Sample	Sample Molar ratio
Cu-BTC-MOF	$1Cu^{2+}/0.556H_3BTC/185H_2O/60EtOH$
Cu-BTC-MOF(0.037 $C_{18\text{-}6\text{-}18}$)	$1Cu^{2+}/0.556H_3BTC/0.037C_{18\text{-}6\text{-}18}/185H_2O/60EtOH$
Cu-BTC-MOF($C_{18\text{-}6\text{-}18}$)	$1Cu^{2+}/0.556H_3BTC/0.075C_{18\text{-}6\text{-}18}/185H_2O/60EtOH$
Cu-BTC-MOF(0.15 $C_{18\text{-}6\text{-}18}$)	$1Cu^{2+}/0.556H_3BTC/0.15C_{18\text{-}6\text{-}18}/185H_2O/60EtOH$
Cu-BTC-MOF(0.30 $C_{18\text{-}6\text{-}18}$)	$1Cu^{2+}/0.556H_3BTC/0.30C_{18\text{-}6\text{-}18}/185H_2O/60EtOH$
Cu-BTC-MOF(0.075 CTMABr)	$1Cu^{2+}/0.556H_3BTC/0.075$ CTMABr $/185H_2O/60EtOH$
Cu-BTC-MOF(CTMABr)	$1Cu^{2+}/0.556H_3BTC/0.15$CTMABr$/185H_2O/60EtOH$
Cu-BTC-MOF($C_{18\text{-}6\text{-}18}$-TMB)	$1Cu^{2+}/0.556H_3BTC/0.075C_{18\text{-}6\text{-}18}/0.075$TMB $/185H_2O/60EtOH$

^{1}HNMR of ([$C_{18}H_{37}$-$N^+(CH_3)_2$-$(CH_2)_6$-$N^+(CH_3)_2$-$C_{18}H_{37}$]2Br^-):

In-depth NMR characterization data are provided here for the $C_{18\text{-}6\text{-}18}$ which is found to be the best suited template investigated in this study. ^{1}H, spectra are shown here to illustrate the formation of $C_{18\text{-}6\text{-}18}$ (Fig. S1). NMR spectra shown here also contain DMSO and H2O signals arising from the deuterated solvent in which these organic compounds were dissolved. The triplet signal at 0.79−0.83 ppm in the ^{1}H NMR spectrum (Fig. S1) is due to the terminal −CH3 protons (designated as "a"). The proton of alkyl chain attached to N ("e, e1", (N−CH2)) are observed at 3.20 ppm with triplet splitting, whereas $-CH_3$ protons attached to quaternary ammonium group (designated as "d") are observed downfield at 2.95 ppm. Similarly the proton of alkyl chain (designated as "b" and "c") are observed at 1.15−1.32 and 1.55−1.65 ppm respectively with multiplet.

^{1}HNMR (DMSO) : δ = 3.20 (m, 8H), 2.95 (s, 12H), 1.55−1.65(m, 8H), 1.15−1.32 (m, 64H), 0.79−0.83 ppm (t, 6H).

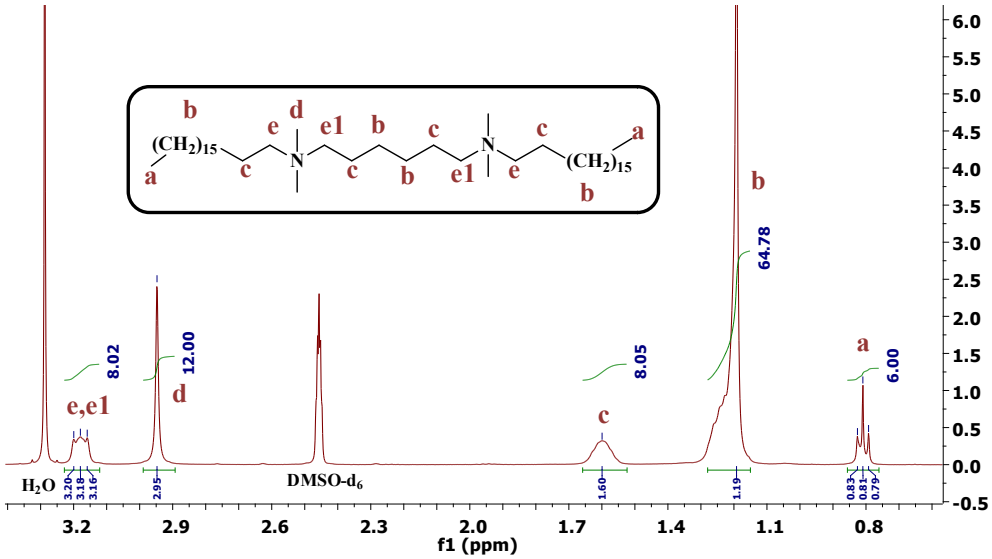

Fig. S1. ^{1}H NMR spectrum of ([$C_{18}H_{37}$-$N^+(CH_3)_2$-$(CH_2)_6$-$N^+(CH_3)_2$-$C_{18}H_{37}$]2Br^-).

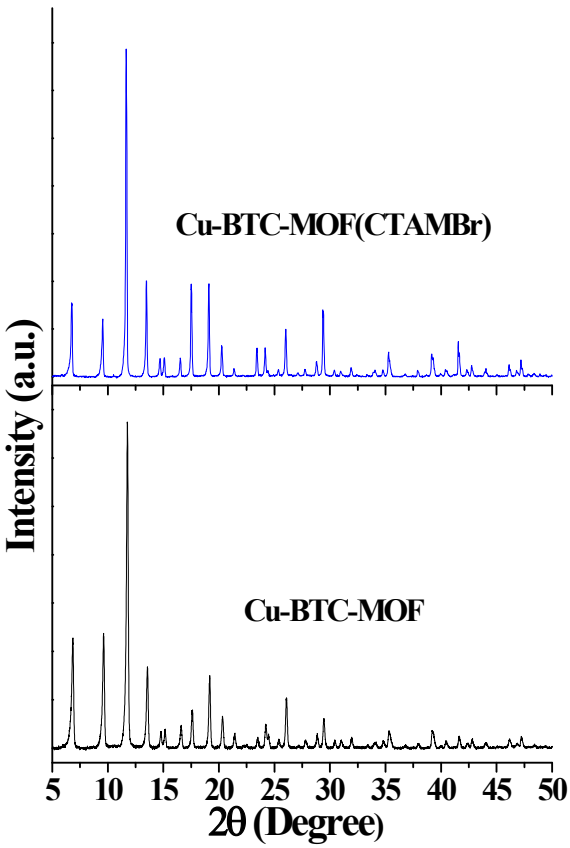

Fig. S2. Powder X-ray diffraction patterns of Cu-BTC-MOF and Cu-BTC-MOF(CTMABr) materials prepared in this study.

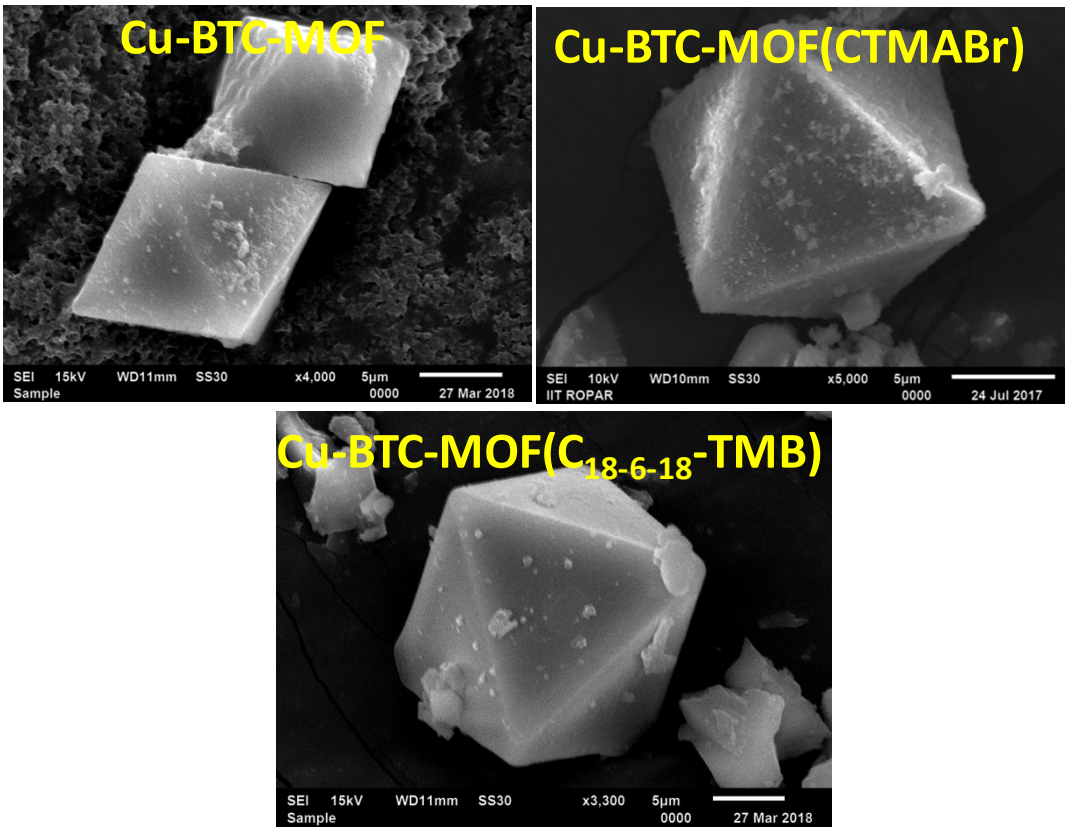

Fig. S3. SEM images of different materials prepared in this study.

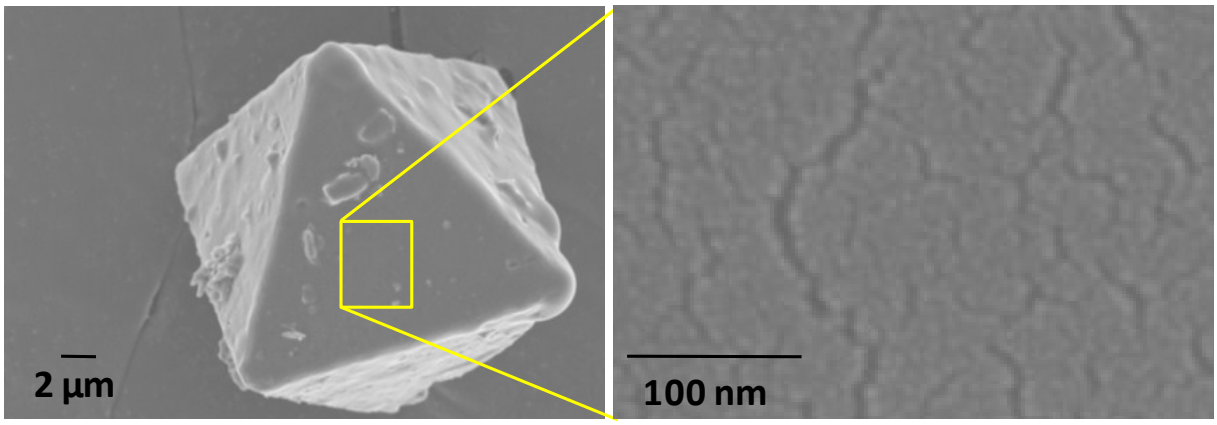

Fig. S4. FE-SEM images of as-synthesized Cu-BTC-MOF($C_{18\text{-}6\text{-}18}$).

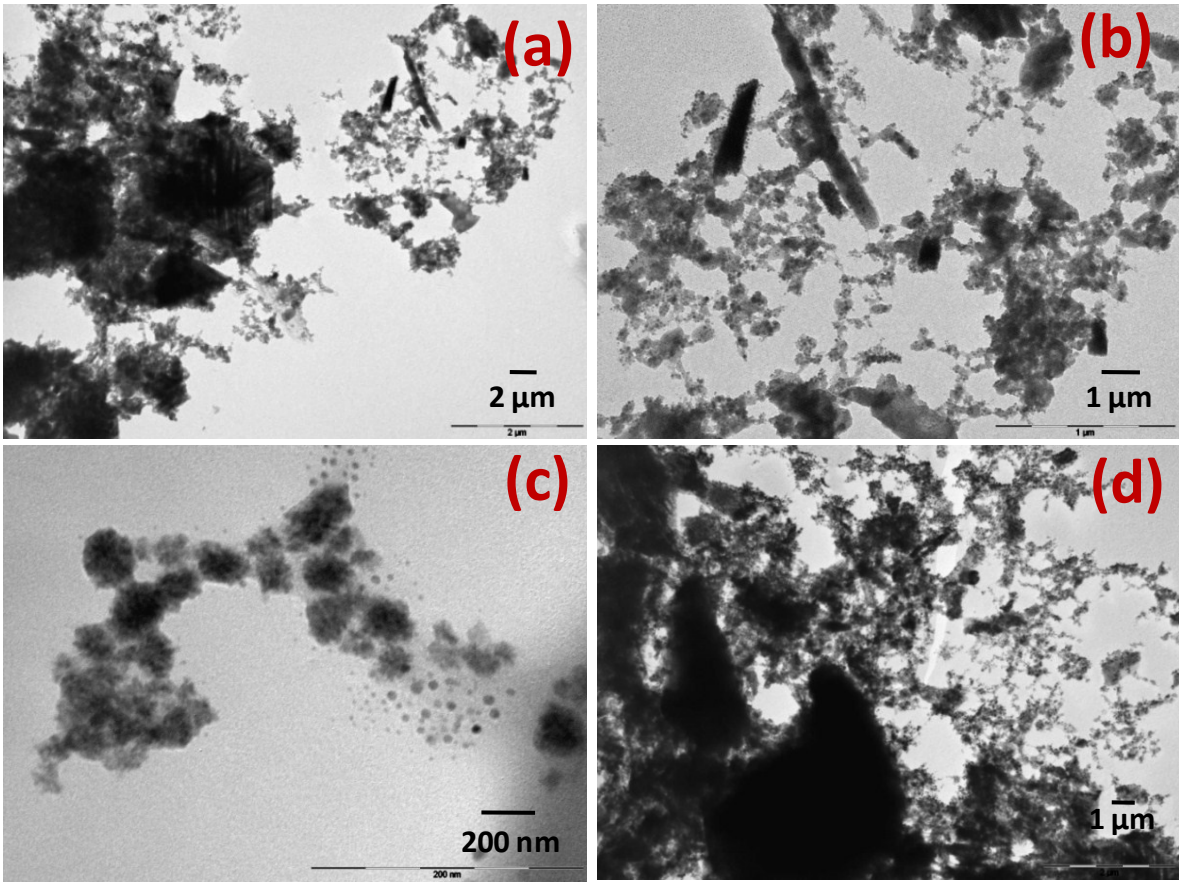

Fig. S5. TEM images of (a-b) Cu-BTC-MOF($C_{18\text{-}6\text{-}18}$), and (c,d) Cu-BTC-MOF($C_{18\text{-}6\text{-}18}$-TMB).

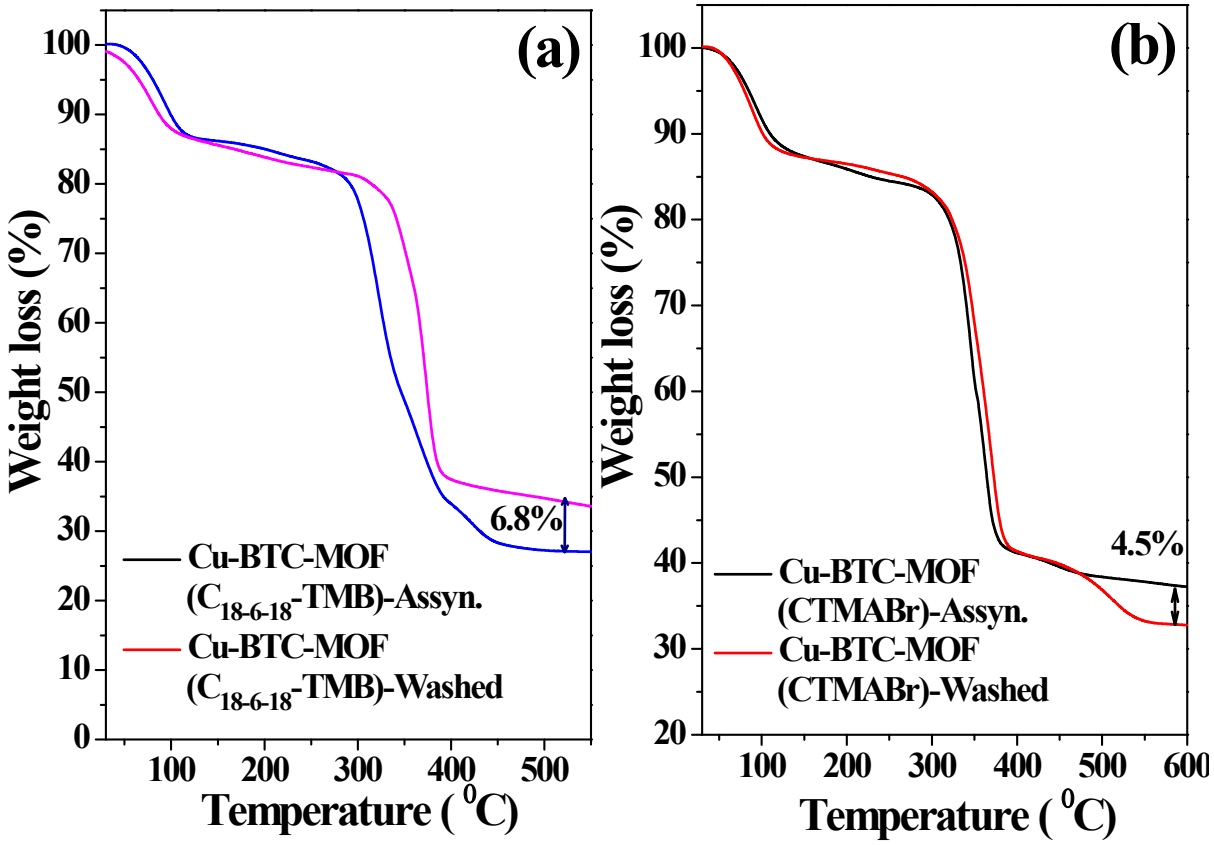

Fig. S6. Thermogravimetric analysis of (a) as-synthesized and after the surfactant removal of Cu-BTC-MOF($C_{18-6-18}$-TMB), and (b) Cu-BTC-MOF(CTMABr).

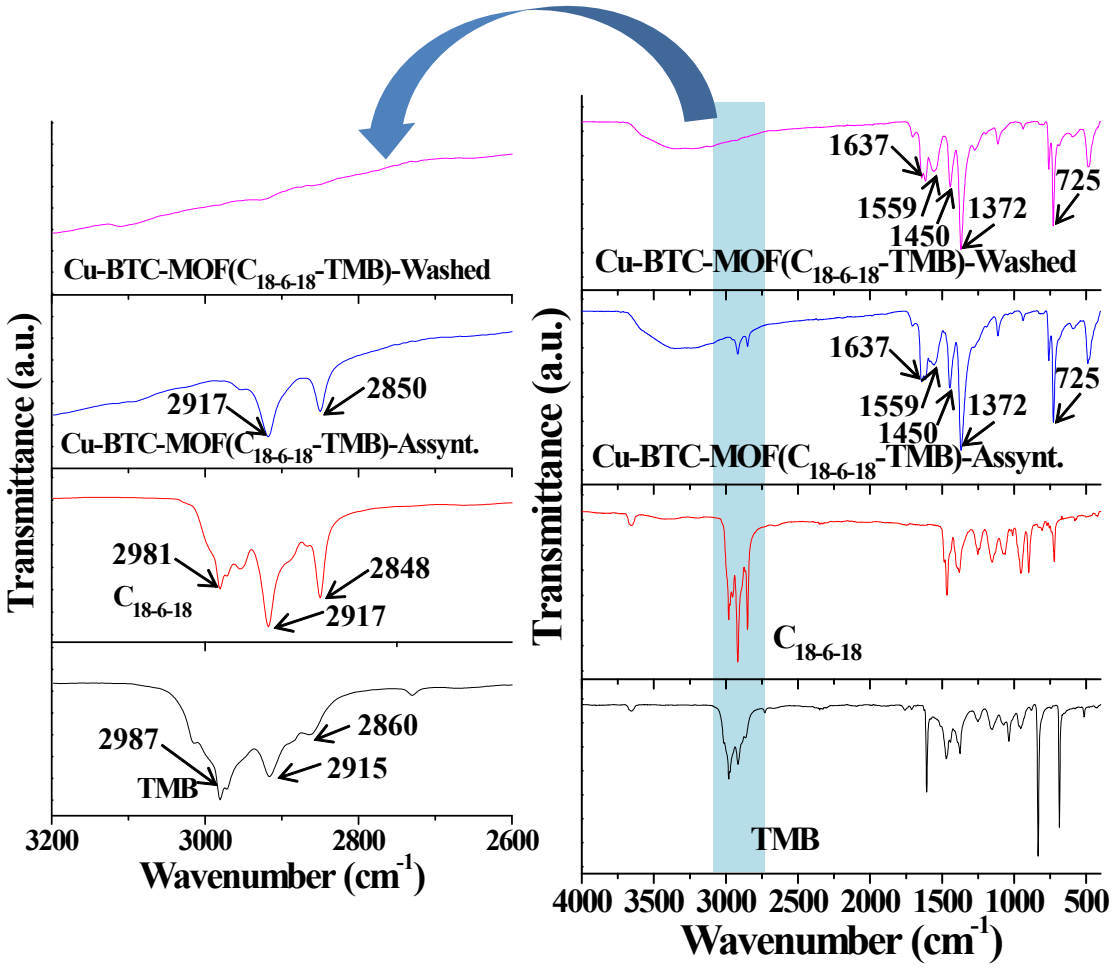

Fig. S7. FT-IR spectra of $C_{18\text{-}6\text{-}18}$, TMB, and Cu-BTC-MOF($C_{18\text{-}6\text{-}18}$-TMB) as-synthesized and after the $C_{18\text{-}6\text{-}18}$ and TMB removal.

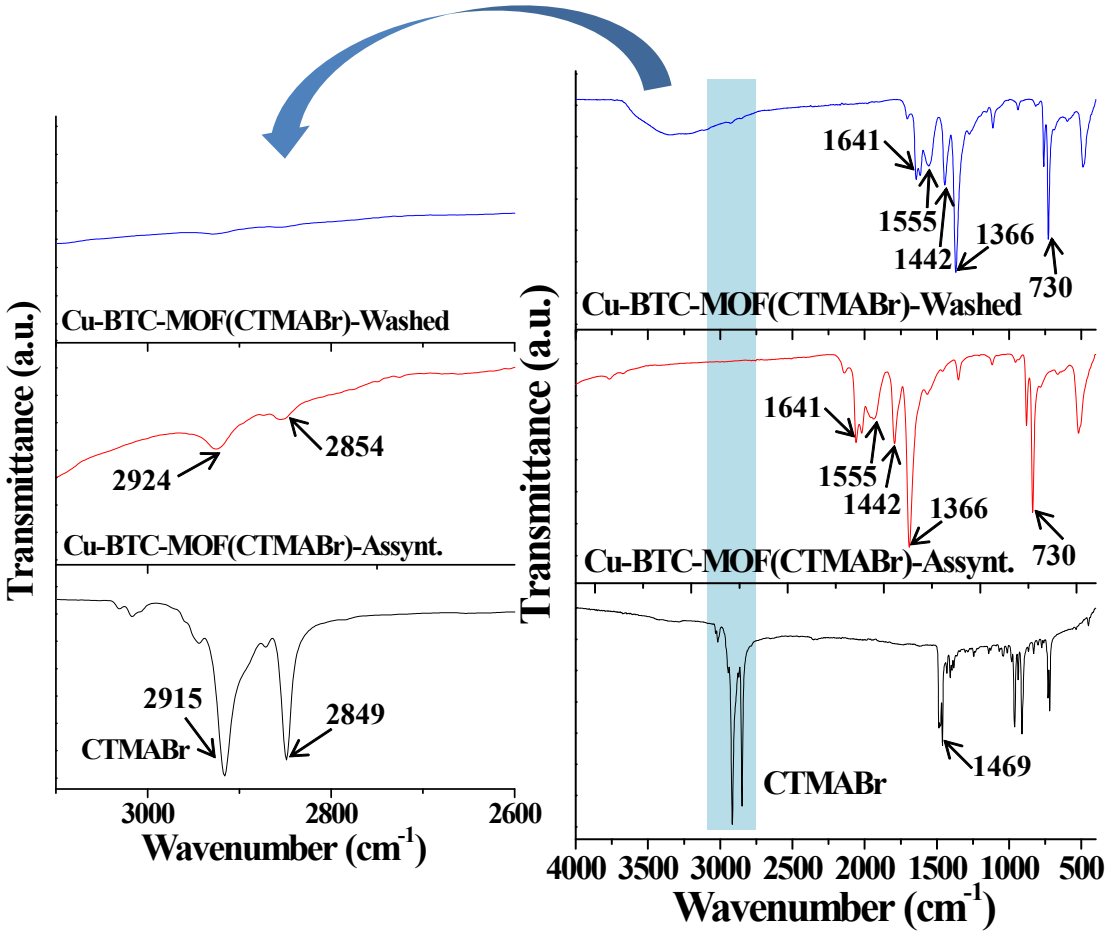

Fig. S8. FT-IR spectra of CTMABr and Cu-BTC-MOF(CTMABr) as-synthesized and after the CTMABr removal.

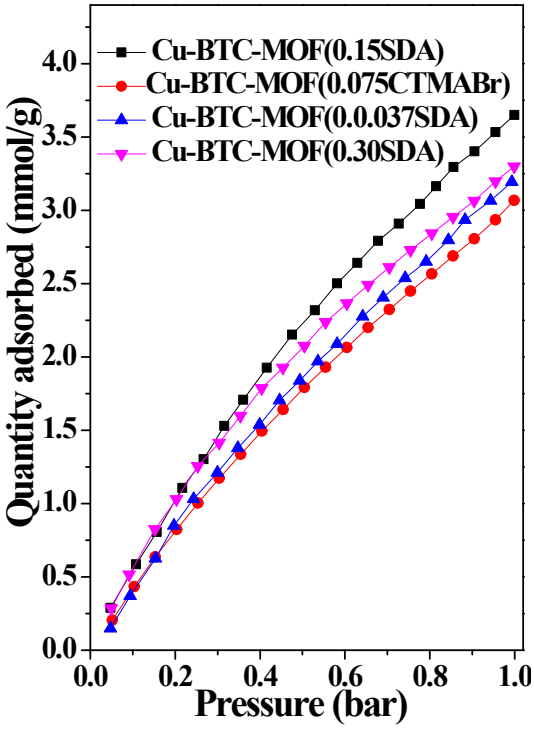

Fig. S9. CO_2 adsorption isotherms of different materials prepared in this study at 25 °C.

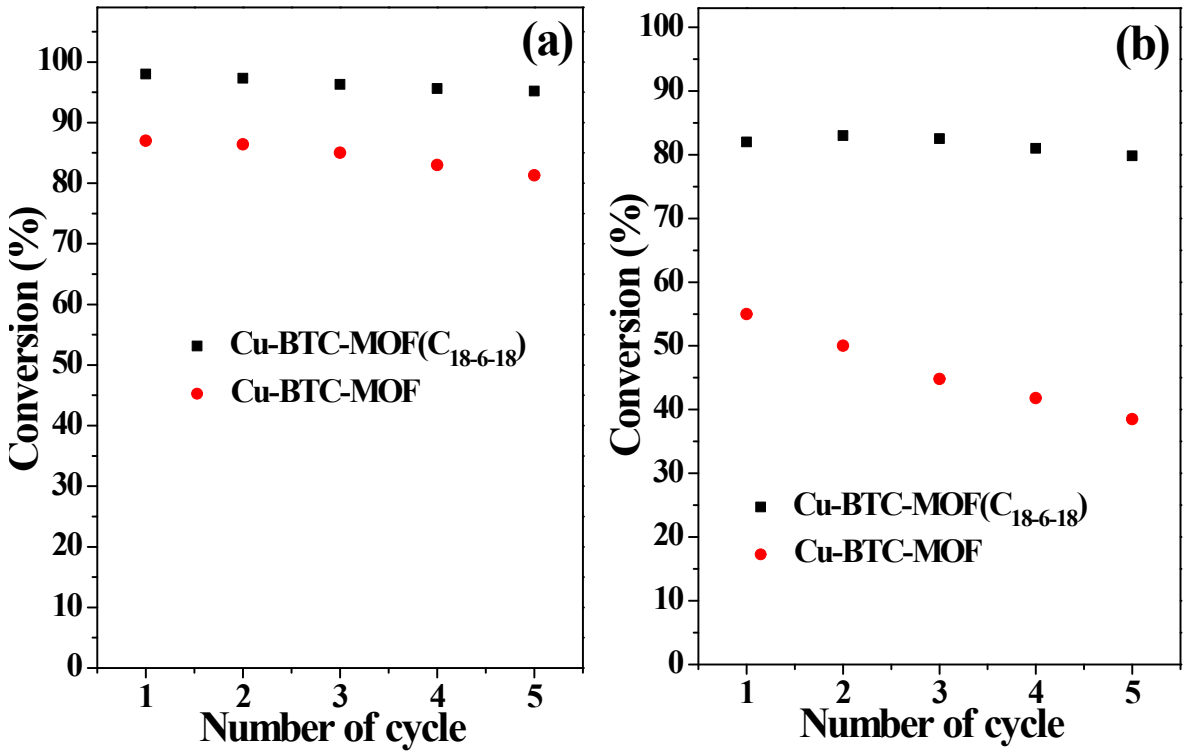

Fig. S10. Reusability of Cu-BTC-MOF($C_{18\text{-}6\text{-}18}$) and Cu-BTC-MOF in the aerobic oxidation of (a) benzyl alcohol, and (b) cinnamyl alcohol, respectively.